NACA TN 3532

NATIONAL ADVISORY COMMITTEE FOR AERONAUTICS

TECHNICAL NOTE 3532

LOW-SPEED STATIC LATERAL AND ROLLING STABILITY CHARACTERISTICS OF A SERIES OF CONFIGURATIONS COMPOSED OF INTERSECTING TRIANGULAR PLAN-FORM SURFACES

By David F. Thomas, Jr.

Langley Aeronautical Laboratory
Langley Field, Va.

Washington
October 1955

1E

NATIONAL ADVISORY COMMITTEE FOR AERONAUTICS

TECHNICAL NOTE 3532

LOW-SPEED STATIC LATERAL AND ROLLING STABILITY CHARACTERISTICS OF A SERIES OF CONFIGURATIONS COMPOSED OF INTERSECTING TRIANGULAR PLAN-FORM SURFACES

By David F. Thomas, Jr.

SUMMARY

The static lateral and rolling stability derivatives of a series of cruciform, inverted T-, V-, and Y-configurations composed of low-aspect-ratio triangular surfaces have been obtained at low speed in the 6-foot-diameter rolling-flow test section of the Langley stability tunnel. These derivatives are presented as functions of the geometry of the models, and for two configurations (a planar wing and an inverted T), as functions of angle of attack. Where possible, comparisons have been made to indicate the extent of agreement between experiment and existing theory. In general, the sideslip derivatives showed better agreement between theory and experiment than the rolling derivatives.

INTRODUCTION

With the trend of modern high-speed aircraft, particularly missiles, toward the use of tail configurations incorporating surfaces of small aspect ratio, a number of theoretical papers have been published on the determination of the stability characteristics of this type of configuration (refs. 1 to 6). Although most of these papers are concerned primarily with supersonic flow, some, which are based on slender-body theory (i.e., thin wings of extremely low aspect ratio and slender bodies), are applicable to subsonic speeds. The theoretical stability characteristics for some tail configurations have been verified experimentally; however, only meager or no experimental data exist for a range of V-, Y-, and cruciform-tail configurations, particularly at low speeds.

The purpose of the present investigation was to obtain experimental data on V-, Y-, and cruciform tails and to compare the data where practical with existing slender-body theory. It should be kept in mind that the slender-body theory treats the case in which the surface carries a finite load at the trailing edge; whereas for the low-speed experimental

conditions used in this investigation, the trailing edge carries no load. Therefore, the theoretical and experimental curves should be compared for trends and not for absolute values.

SYMBOLS

The symbols used in this paper are referred to the stability system of axes with the origin of the axes located at two-thirds of the model root chord. Positive directions of forces, moments, and displacements about the stability axes are shown in figure 1.

b span, ft

S area, sq ft

c_r root chord, ft

D diameter of circle swept by surface, ft

F_Y lateral force

M_X rolling moment

M_Z yawing moment

q dynamic pressure, lb/sq ft

V free-stream velocity, ft/sec

x/c_r longitudinal location of lateral-force center of pressure in percent of root chord

α angle of attack, deg

β angle of sideslip, deg

Γ dihedral angle, deg

p rolling angular velocity, radians/sec

C_Y lateral-force coefficient, $\frac{\text{Lateral force}}{qS}$

$$(C_Y)_{TT} = \frac{\text{Lateral force}}{q(\text{Area of vertical surface})}$$

$$(C_Y)_{CT} = \frac{\text{Lateral force}}{q(\text{Total area of vertical surfaces})}$$

$$(C_Y)_{VT} = \frac{\text{Lateral force}}{2q(\text{Area of one surface of V-configuration})}$$

$$(C_Y)_{YT} = \frac{\text{Lateral force}}{2q(\text{Area of one surface of V-portion of configuration})}$$

C_n yawing-moment coefficient, $\frac{\text{Yawing moment}}{qSb}$

$$(C_n)_{TT} = \frac{\text{Yawing moment}}{q(\text{Area of vertical surface})(\text{Span of vertical surface})}$$

$$(C_n)_{CT} = \frac{\text{Yawing moment}}{q\left(\begin{array}{c}\text{Total area of}\\ \text{vertical surfaces}\end{array}\right)\left(\begin{array}{c}\text{Total span of}\\ \text{vertical surfaces}\end{array}\right)}$$

$$(C_n)_{VT} = \frac{\text{Yawing moment}}{4q\left(\begin{array}{c}\text{Area of one surface of}\\ \text{V-configuration}\end{array}\right)\left(\begin{array}{c}\text{Span of one surface of}\\ \text{V-configuration}\end{array}\right)}$$

$$(C_n)_{YT} = \frac{\text{Yawing moment}}{4q\left(\begin{array}{c}\text{Area of one surface of}\\ \text{V-portion of configuration}\end{array}\right)\left(\begin{array}{c}\text{Span of one surface of}\\ \text{V-portion of configuration}\end{array}\right)}$$

C_l rolling-moment coefficient, $\frac{\text{Rolling moment}}{qSb}$

$$(C_l)_{TT} = \frac{\text{Rolling moment}}{q(\text{Area of vertical surface})(\text{Span of vertical surface})}$$

$$(C_l)_{CT} = \frac{\text{Rolling moment}}{q(\text{Total area of vertical surfaces})(\text{Total span of vertical surfaces})}$$

$$(C_l)_{VT} = \frac{\text{Rolling moment}}{4q\left(\begin{array}{c}\text{Area of one surface of}\\ \text{V-configuration}\end{array}\right)\left(\begin{array}{c}\text{Span of one surface of}\\ \text{V-configuration}\end{array}\right)}$$

$$(C_l)_{YT} = \frac{\text{Rolling moment}}{4q\left(\begin{array}{c}\text{Area of one surface of}\\ \text{V-portion of configuration}\end{array}\right)\left(\begin{array}{c}\text{Span of one surface of}\\ \text{V-portion of configuration}\end{array}\right)}$$

$\frac{pb}{2V}$ path helix angle, radians

$$\left(\frac{pb}{2V}\right)_{TT} = \frac{p}{2V}\,(\text{Span of vertical surface})$$

$$\left(\frac{pb}{2V}\right)_{CT} = \frac{p}{2V}\,(\text{Total span of vertical surfaces})$$

$$\left(\frac{pb}{2V}\right)_{VT} = \frac{p}{2V}\,(\text{Twice span of one surface of V-configuration})$$

$$\left(\frac{pb}{2V}\right)_{YT} = \frac{p}{2V}\,(\text{Twice span of one surface of V-portion of configuration})$$

$$C_{Y_\beta} = \frac{\partial C_Y}{\partial \beta} \text{ per degree}$$

$$C_{n_\beta} = \frac{\partial C_n}{\partial \beta} \text{ per degree}$$

$$C_{l_\beta} = \frac{\partial C_l}{\partial \beta} \text{ per degree}$$

$$C_{Y_p} = \frac{\partial C_Y}{\partial \frac{pb}{2V}} \text{ per radian}$$

$$C_{n_p} = \frac{\partial C_n}{\partial \frac{pb}{2V}} \text{ per radian}$$

$$C_{l_p} = \frac{\partial C_l}{\partial \frac{pb}{2V}} \text{ per radian}$$

Subscripts:

H horizontal surface

V vertical surface

u upper

l lower

CT cruciform configuration

TT inverted T-configuration

VT V-configuration

YT Y-configuration

MODELS AND TESTS

The models used in this investigation were assembled of plywood half-delta surfaces having rounded leading edges and tapered trailing edges. (See fig. 2(a).) The surfaces had root chords of 4.12 feet and semispans ranging from 0.375 to 1.875 feet.

The various configurations were obtained by clamping the surfaces to a mounting rod slightly less in diameter than the thickness of the plywood. The intersections between surfaces were then sealed. The models were assembled in such a manner that the apexes of all surfaces were coincident and their trailing edges were in a plane normal to the line of intersection. The line of intersection coincided with the root chords of

the surfaces. The complete range of configurations is indicated in figures 2(b) and 2(c), and two of the configurations tested in this investigation are shown in figure 3.

The models were mounted on a single strut support system with the mounting point at two-thirds of the root chord measured from the apex of the model. All models were mounted upright as indicated in figures 2(b), 2(c), and 3(a) with the exception of the Y-configurations which were tested in an inverted position as shown in figure 3(b). Forces and moments were measured by a six-component balance system.

The tests were made in the 6-foot-diameter rolling-flow test section of the Langley stability tunnel at a dynamic pressure of 39.7 pounds per square foot, which corresponds to a Mach number of 0.164 and a Reynolds number of approximately 4.8×10^6 based on the root chord of the surfaces of 4.12 feet.

Sideslip data were obtained for values of sideslip angle β equal to 0°, $\pm 2^\circ$, and $\pm 5^\circ$. Rolling-stability data were obtained by using values of $p/2V$ of 0, ± 0.005, ± 0.010, and ± 0.015 radian per foot of span. In most cases, the angle of attack was set at 0°; however, two configurations - the 3-foot-span planar surface and the inverted T-configuration, having a horizontal-surface span equal to 1.5 feet and a ratio of horizontal-surface span to vertical-surface span b_H/b_V equal to 1 - were tested at angles of attack up to 26°.

In order to determine the effect of thickness on the lift-curve slope of the surfaces, two delta wings having the same sweep angle of the leading edge of 84.8° and having thicknesses of 3/8 inch and 3/4 inch were tested through an angle-of-attack range. It was felt that a comparison of the results obtained from these two wings would give an indication of the validity of eliminating thickness effects as a factor in comparing the results obtained using the 3/4-inch-thick surfaces with the slender-body theoretical results wherein the surfaces are assumed to have zero thickness. The effects of thickness for the surfaces tested were found to be small.

Corrections have been applied for jet-boundary effects on angles of attack and sideslip according to the method presented in reference 7. Tare corrections have been applied to the rolling-flow data of the cruciform configurations in an attempt to eliminate the effect of the cutout in the lower vertical surface necessitated by the method of mounting the models.

It is possible for a slight misalinement of the roll axis of the tunnel flow to produce increments of the side-force derivative C_{Y_p} as evidenced in the results for the cruciform configuration $\left(b_{V_l}/b_{V_u} = 1.00\right)$ at 0° angle of attack and for the planar configuration at 0° angle of attack. No attempt has been made to correct for this effect.

RESULTS AND DISCUSSION

Sideslip Characteristics

Cruciform configurations.- The measured sideslip characteristics for the cruciform configurations are shown in figure 4 as curves of the derivatives C_{Y_β}, C_{n_β}, and C_{l_β} plotted against the ratio of horizontal span to vertical span b_H/b_V for several values of the ratio of the lower span to the upper span of the vertical surface b_{V_l}/b_{V_u}.

The experimental results show that, for the inverted T-arrangement $\left(b_{V_l}/b_{V_u} = 0\right)$, the derivatives C_{Y_β} and C_{n_β} increased negatively almost linearly with the ratio b_H/b_V until a value of b_H/b_V of about 1.0 was reached. Further increases in the ratio caused little change in C_{n_β}, whereas the negative slope of C_{Y_β} was slightly decreased. The derivative C_{l_β} remained nearly constant until the ratio of horizontal-surface span to vertical-surface span of 1.0 was reached; then it decreased with further increase in b_H/b_V. The effects of horizontal-tail span indicated herein for the inverted T-configurations, usually referred to as end-plate effects, are qualitatively the same as those shown by the theoretical and experimental data of reference 8 and the theoretical analysis of reference 9 even though these references are concerned with aspect ratios and sweep angles very different from those of the present investigation. Equations presented in reference 4 are directly applicable to the inverted T-configurations and were used to obtain the variation of C_{Y_β} and C_{l_β} with b_H/b_V. The results are presented in figure 4 for comparison with the experimental data. The agreement between theory and experiment is good for both C_{Y_β} and C_{l_β}.

The effect of varying the vertical position of the horizontal surface $\left(\text{increasing } b_{V_l}/b_{V_u}\right)$ was to decrease the end-plate effect on C_{Y_β} and C_{l_β} for all ratios of b_H/b_V. The results also indicate that the rate of change of end-plate effect with increasing b_{V_l}/b_{V_u} was very great when the horizontal surface was near the base of the vertical surface $\left(b_{V_l}/b_{V_u} = 0\right)$, but became negligible as the horizontal surface neared the center of the vertical surface $\left(b_{V_l}/b_{V_u} = 1.0\right)$. These effects are consistent with those of reference 8.

The effects of variation of angle of attack on the sideslip derivatives for a planar delta wing and an inverted T-configuration are presented in figure 5. Below an angle of attack of approximately 6°, the sideslip derivatives C_{Y_β} and C_{n_β} were nearly equal to zero for the planar configuration. This and the variation of C_{l_β} up to an angle of attack of approximately 16° are in agreement with the theory of reference 5. The addition of a vertical surface on top of the planar configuration produced negative increments of all three derivatives at 0° angle of attack. A comparison of the data of figures 5(a) and 5(b) shows that the negative increment in the case of C_{n_β} decreased considerably as the angle of attack was increased.

V-configurations.- The measured sideslip characteristics of the V-configurations (see fig. 2(b)) are shown in figure 6 as curves of C_{Y_β}, C_{n_β}, and C_{l_β} plotted against dihedral angle. The results indicated a nearly linear increase in the negative values of C_{Y_β} and C_{n_β} for the range of dihedral angle from 15° to 60°. Between dihedral angles of 0° and 15°, C_{Y_β} and C_{n_β} showed only slight negative increases. The variation of C_{l_β} with increasing dihedral angle from 0° to 60° was nearly linear and negative. This variation of C_{l_β} is in good agreement with the results of reference 5 in the range of small dihedral angles for which this theory is applicable.

Y-configurations.- The addition of vertical members to the bottom of the 45° dihedral-angle V-configuration, forming a Y-configuration, produced negative increments in C_{Y_β} and C_{n_β} which increased as the ratio b_V/D was increased. (See fig. 7.) Increasing the span of the vertical surface of the Y-configuration caused little change in C_{l_β} for b_V/D ratios up to about 0.4. Further increases in b_V/D caused C_{l_β} to become less negative.

Centers of pressure.- Figure 8 presents the longitudinal location of the lateral-force centers of pressure for the various configurations tested. All configurations tested are in fairly good agreement with slender-body theory except the planar delta surface at angles of attack other than zero.

Steady Rolling Characteristics

Cruciform configurations.- The measured steady rolling characteristics for the cruciform configurations are shown in figure 9 as curves of the

derivatives C_{Y_p}, C_{n_p}, and C_{l_p} plotted against the ratio of horizontal span to vertical span b_H/b_V for several values of the ratio of the lower span to the upper span of the vertical surface b_{V_l}/b_{V_u}.

The experimental results indicated, in general, a decrease in the negative values of C_{Y_p} for increases in the span of the horizontal surface. The rolling derivative C_{l_p} exhibited an increase in negative values with increased horizontal span. No definite trend was indicated in C_{n_p}.

The effect of varying the vertical location of the horizontal member $\left(\text{increasing } b_{V_l}/b_{V_u}\right)$ was to decrease the negative values of C_{Y_p} and C_{l_p} for all ratios of horizontal-surface span to vertical-surface span b_H/b_V. The theoretical results of reference 4 for C_{l_p} are in good agreement with the experimental results when the horizontal surface is not at the base of the vertical surface. The theory overestimates values for C_{Y_p} and C_{l_p} for the inverted T-configurations.

The effects of variation in angle of attack on the steady rolling stability derivatives for a planar delta and an inverted T-configuration are presented in figure 10. For the planar delta configuration, there is not very good agreement between the theoretical curves of C_{Y_p} and C_{n_p} calculated by reference 5 and the experimental results, and there is only fair agreement between the corresponding theoretical and experimental values of C_{l_p}. The reason for this lack of agreement is not known; however, it is possible that the full theoretical edge suction was not realized experimentally. This factor is the source of the C_{Y_p} and C_{n_p} derivatives and may make C_{l_p} appreciably different from the theoretical results. Some additional tests made in conjunction with this investigation indicated that the upwash of the support strut caused an increment of C_{Y_p} about equal to the amount that the experimental curve of figure 10(a) is displaced from the origin at zero angle of attack.

V-configurations.- The rolling derivatives C_{Y_p}, C_{n_p}, and C_{l_p} for the V-configurations are shown plotted against dihedral angle in figure 11. Up to a dihedral angle of approximately 45°, the most obvious effect of dihedral angle was the negative increase in C_{Y_p}, which was associated with the increase in the projected lateral area of the surfaces. Above a dihedral angle of 45°, the interference between the two semispans tended

to disrupt the trend of C_{Y_p} and caused the slope of C_{Y_p} against Γ to become less negative and to go positive for dihedral angles above 75°. The variation of the experimental derivative C_{n_p} with dihedral angle was about half of that predicted by theory up to a dihedral angle of 45°. From a dihedral angle of 45° to approximately 75°, C_{n_p} remained nearly constant, and at 90°, it decreased slightly from the value at 75°. The derivative C_{l_p} was roughly constant at about -0.1 from 0° to 60° of dihedral, but it decreased thereafter, becoming about one-half the value at the origin for 90° of dihedral. These experimental results are not in good agreement with the theory of reference 4 for C_{Y_p} and C_{l_p} but are in fair agreement with that of reference 5 for C_{Y_p} up to dihedral angles of about 15° and for C_{l_p} up to dihedral angles of about 60°. This difference between theoretical and experimental results may be attributable to a difference in edge suction as mentioned previously in connection with the results for the planar wing at an angle of attack.

Y-configurations.- The effect of variation of the span of a vertical member added to the bottom of a 45° dihedral-angle V-configuration on the steady rolling derivatives C_{Y_p}, C_{n_p}, and C_{l_p} is shown in figure 12. The effect of the addition of small vertical spans, b_V/D less than 0.2, was to increase the negative value of C_{Y_p}. As the vertical member became larger, however, C_{Y_p} became less negative and finally went positive in the region of $b_V/D = 0.6$. The value of the rolling derivative C_{l_p} increased only slightly up to $b_V/D = 0.4$. Beyond this point C_{l_p} became appreciably more negative, being at $b_V/D = 0.6$ about twice the value at the origin. The derivative C_{n_p} was small and little affected by the addition of the lower surface for the range investigated. Agreement between the theoretical results of reference 4 and experiment is not good for C_{Y_p}, C_{n_p}, and C_{l_p}.

Centers of pressure.- Figure 13 presents the longitudinal location of the lateral-force centers of pressure for the various configurations tested in rolling flow. The agreement between the theoretical centers of pressure of references 4 and 5 and the experimental centers of pressure is good to fair for all zero-angle-of-attack cases covered except for the cruciform arrangements having the horizontal surface located in the center of the vertical surface. The planar delta and inverted T-configurations that were tested through a range of angle of attack experienced a loss in side force as the angle of attack was increased which, when combined with the yawing-moment couple existing, gave large

movements of the center of pressure toward the apex. In such cases, the comparison of theoretical and experimental C_{n_p} values as in figure 10(a) is of more significance as a measure of the agreement between theory and experiment.

From 0° to 6° angle of attack, the inverted T-configuration center of pressure is in good agreement with the theory of reference 4. The agreement between theoretical and experimental centers of pressure in this same angle-of-attack range for the planar delta wing is not very good.

CONCLUDING REMARKS

The static lateral and rolling stability derivatives of a series of cruciform, inverted T-, V-, and Y-configurations composed of low-aspect-ratio triangular surfaces have been obtained at low speed in the 6-foot-diameter rolling-flow test section of the Langley stability tunnel. These derivatives are presented as functions of the geometry of the models, and, for two configurations (a planar wing and an inverted T), as functions of angle of attack. These configurations were tested in order to obtain data for comparison with the results of theoretical studies, and where possible, comparisons were made to indicate the extent of agreement between theory and experiment. In general, the sideslip derivatives showed better agreement between theory and experiment than the rolling derivatives, and the derivatives that depended upon the aerodynamic load acting normal to the surface (rolling moment) showed better agreement with theory than the derivatives depending upon edge suction (side force and yawing moment).

Langley Aeronautical Laboratory,
National Advisory Committee for Aeronautics,
Langley Field, Va., July 13, 1955.

REFERENCES

1. Adams, Gaynor J.: Theoretical Damping in Roll and Rolling Effectiveness of Slender Cruciform Wings. NACA TN 2270, 1951.

2. Sacks, Alvin H.: Aerodynamic Forces, Moments, and Stability Derivatives for Slender Bodies of General Cross Section. NACA TN 3283, 1954.

3. Spreiter, John R.: The Aerodynamic Forces on Slender Plane- and Cruciform-Wing and Body Combinations. NACA Rep. 962, 1950. (Supersedes NACA TN's 1897 and 1662.)

4. Bobbitt, Percy J., and Malvestuto, Frank S., Jr.: Estimation of Forces and Moments Due to Rolling for Several Slender-Tail Configurations at Supersonic Speeds. NACA TN 2955, 1953.

5. Ribner, Herbert S.: The Stability Derivatives of Low-Aspect-Ratio Triangular Wings at Subsonic and Supersonic Speeds. NACA TN 1423, 1947.

6. Ribner, Herbert S.: Damping in Roll of Cruciform and Some Related Delta Wings at Supersonic Speeds. NACA TN 2285, 1951.

7. Glauert, H.: The Elements of Aerofoil and Airscrew Theory. Second ed., Cambridge Univ. Press, 1947, pp. 189-198. (Reprinted 1948.)

8. Riley, Donald R.: Effect of Horizontal-Tail Span and Vertical Location on the Aerodynamic Characteristics of an Unswept Tail Assembly in Sideslip. NACA Rep. 1171, 1954. (Supersedes NACA TN 2907.)

9. Queijo, M. J., and Riley, Donald R.: Calculated Subsonic Span Loads and Resulting Stability Derivatives of Unswept and 45° Sweptback Tail Surfaces in Sideslip and in Steady Roll. NACA TN 3245, 1954.

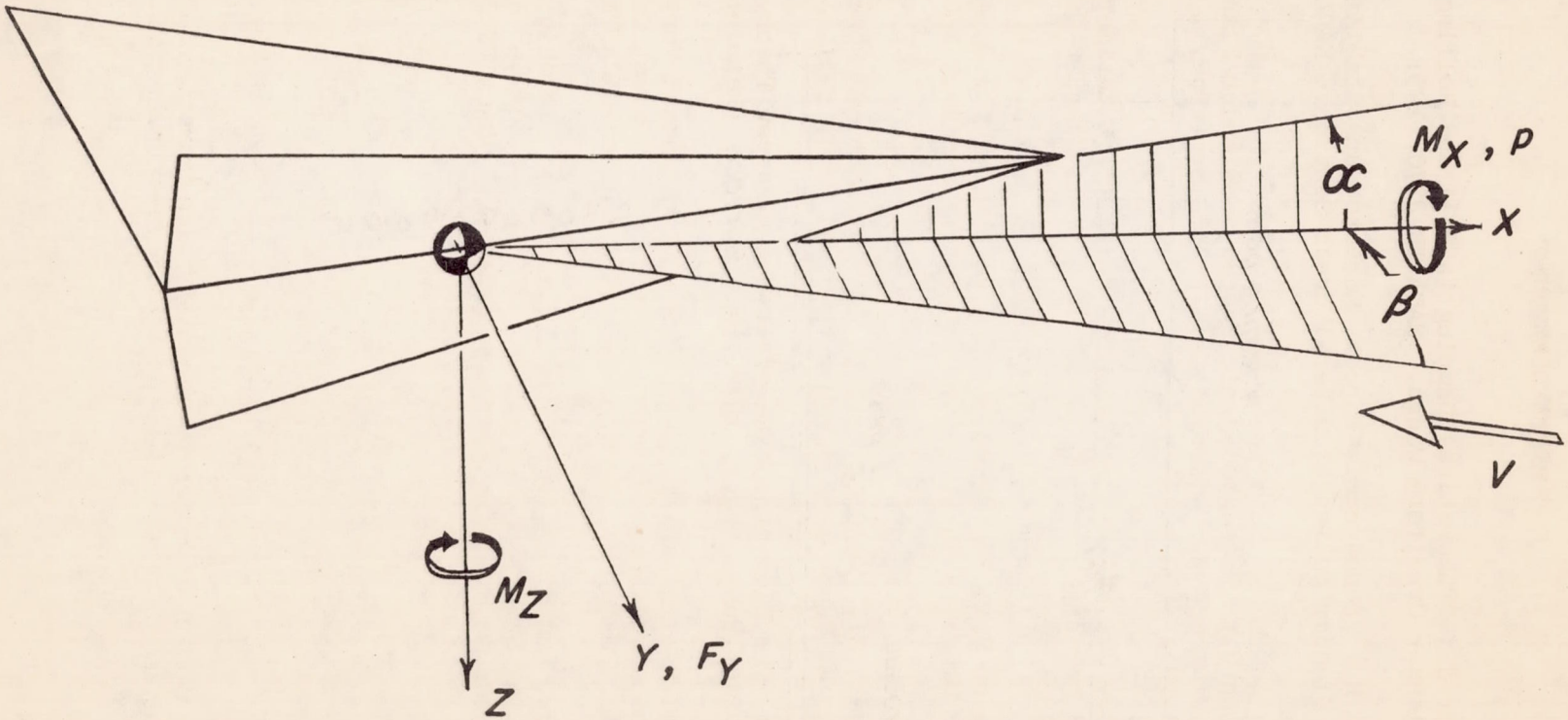

Figure 1.- Stability system of axes. Arrows indicate positive directions of forces, moments, and displacements applied to the model.

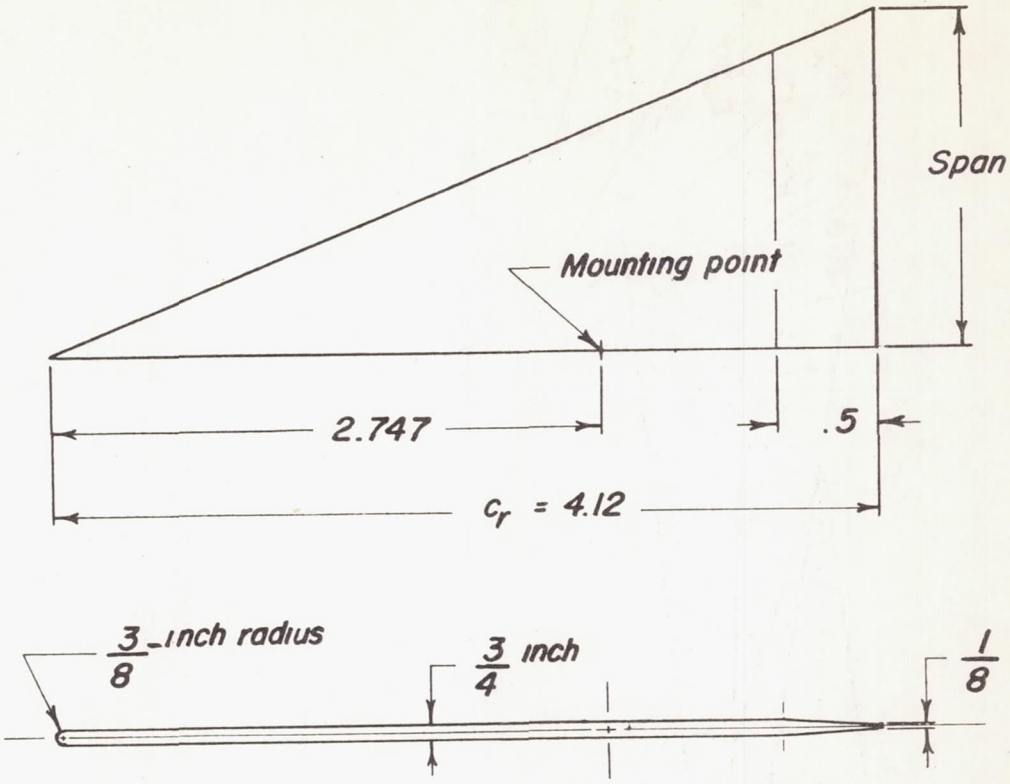

Surface	Span, ft
P_1	0.375
P_2	.50
P_3	.75
P_4	1.00
P_5	1.125
P_6	1.500
P_7	1.875

(a) Surfaces.

Figure 2.- Sketch of model surfaces and configurations used in investigation. All dimensions are in feet unless otherwise specified.

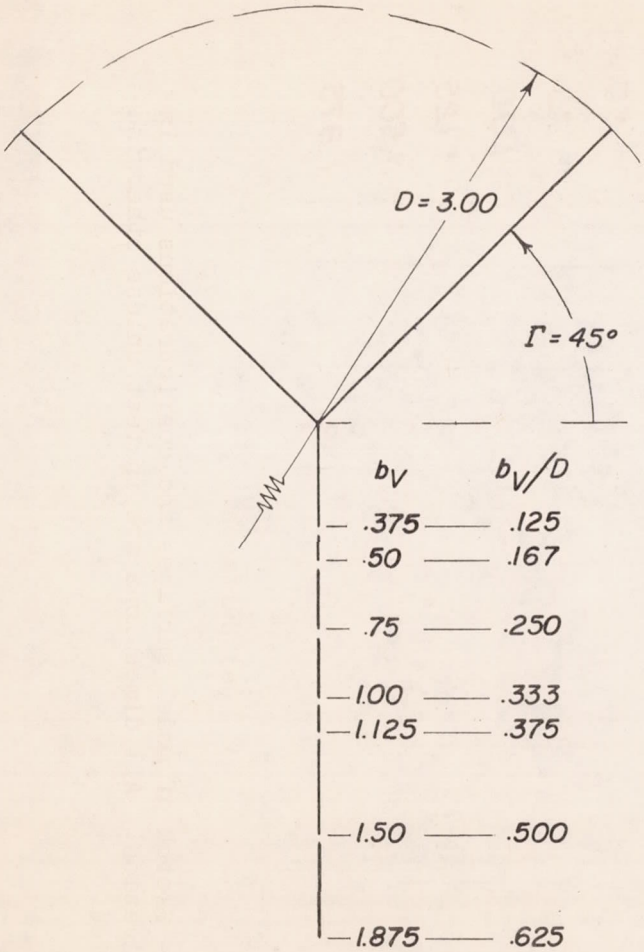

Y - configuration

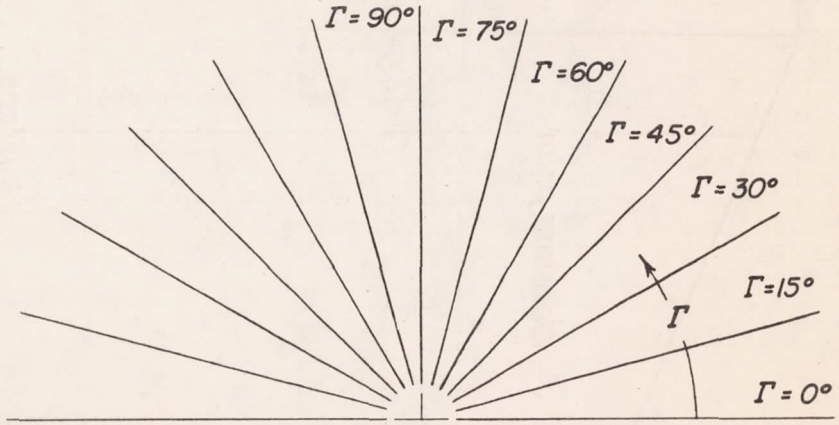

Planar and V - configurations; b = 3.00 ft

(b) Cross sections of configurations at trailing edges.

Figure 2.- Continued.

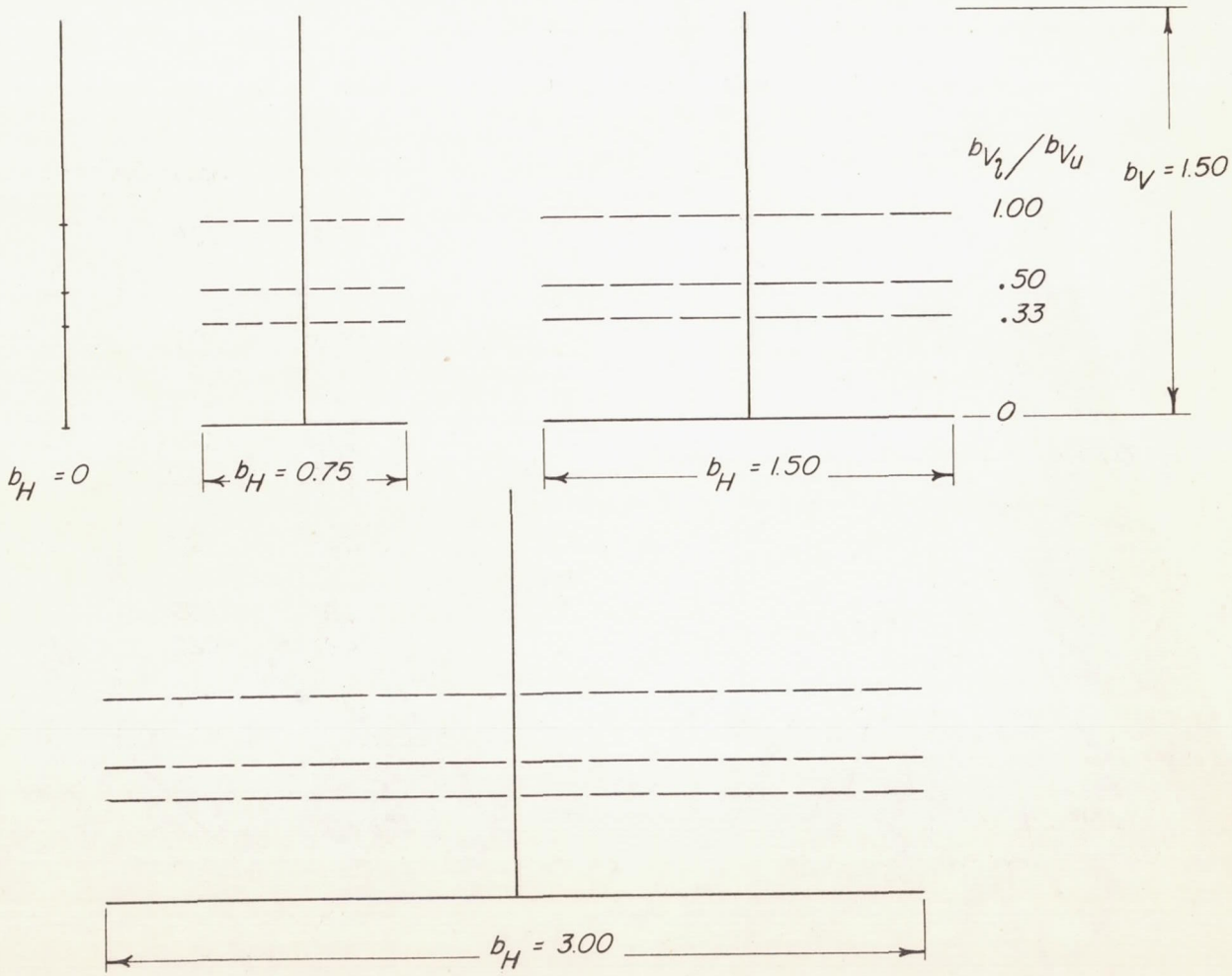

(c) Cross sections of inverted T- and cruciform configurations at trailing edges.

Figure 2.- Concluded.

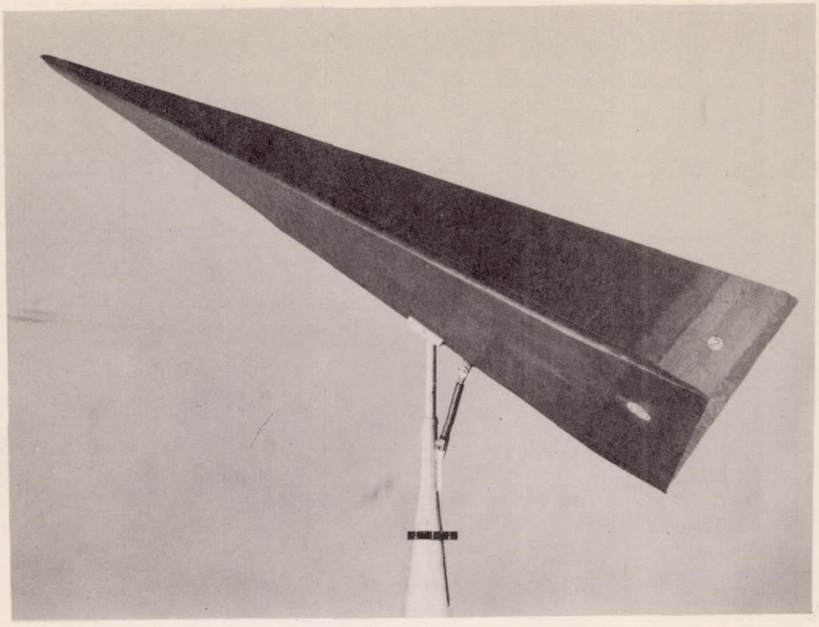

(a) V-configuration.

L-79686

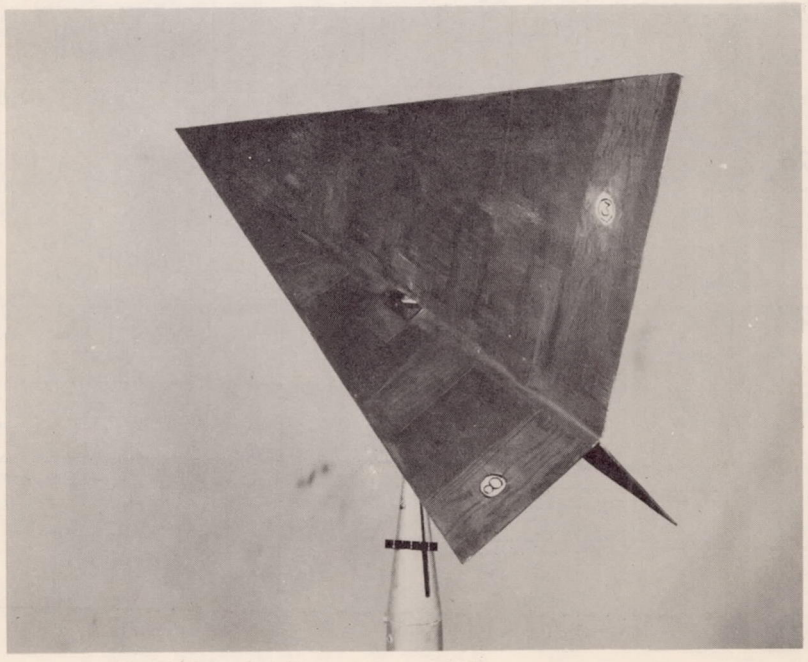

(b) Y-configuration.

L-79687

Figure 3.- Representative configurations.

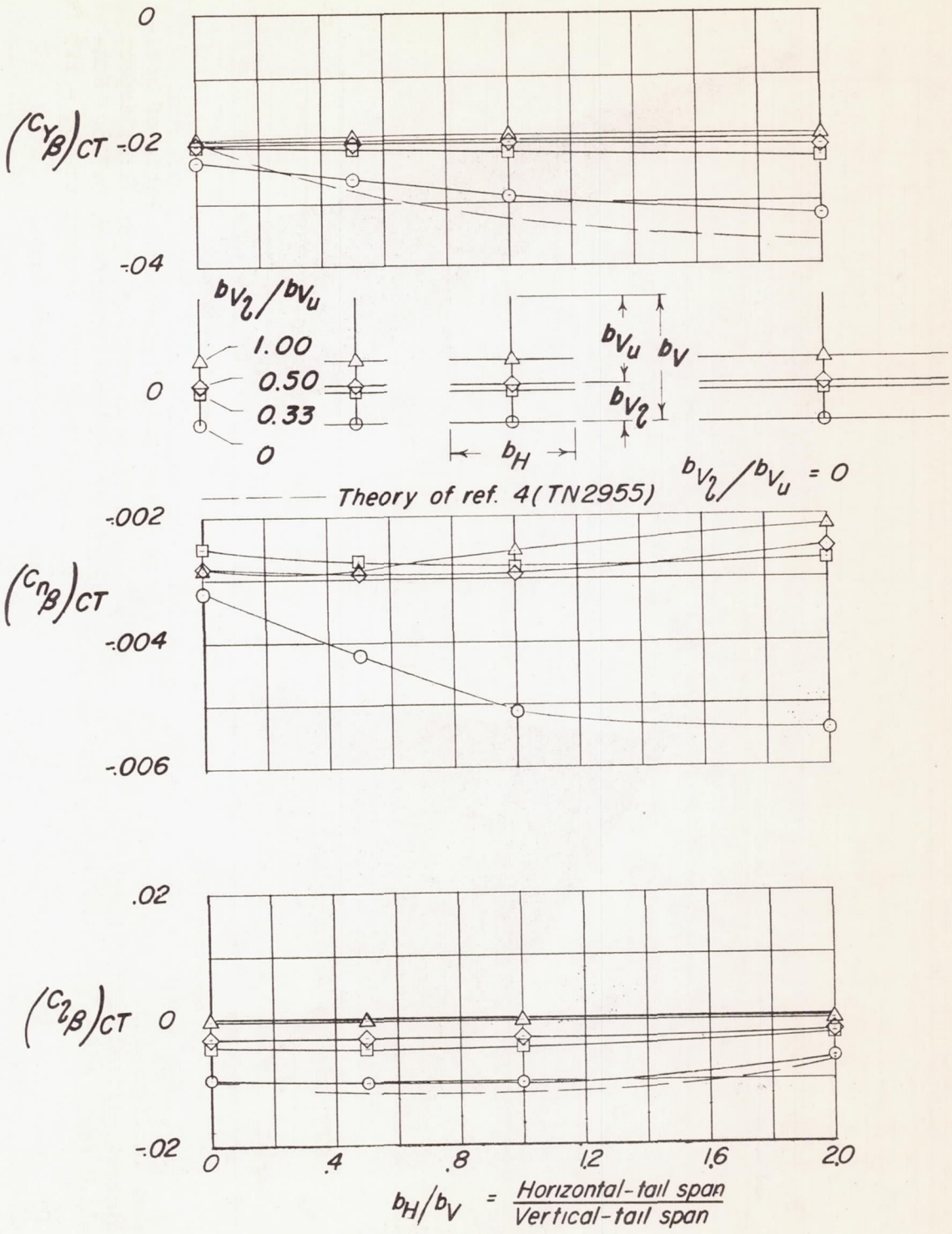

Figure 4.- Effect of ratio of lower to upper vertical span on the sideslip derivatives for a series of cruciform configurations. b_V = 1.5 feet; S_V = 3.09 square feet.

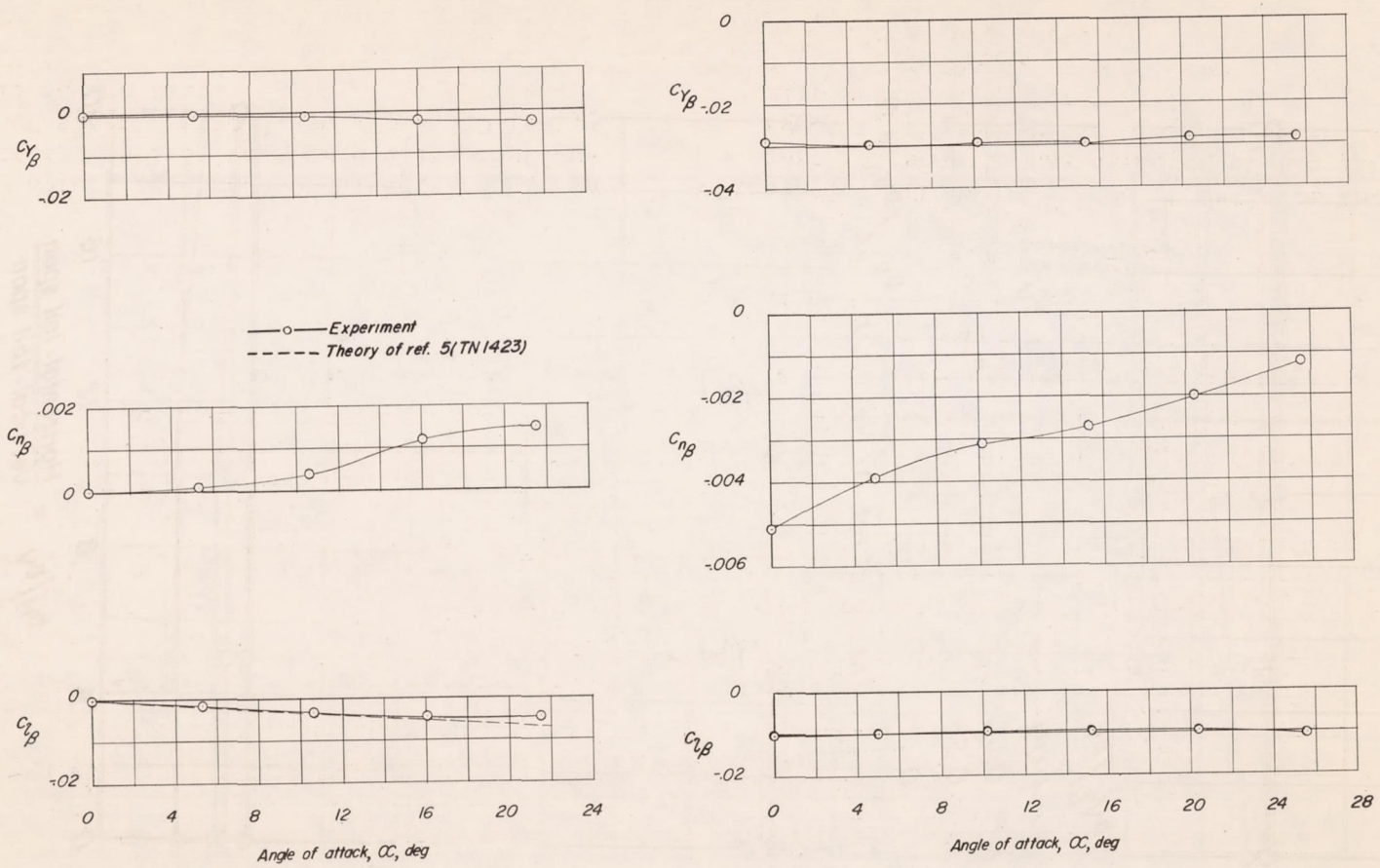

(a) Planar configuration. Aspect ratio, 1.456. Nondimensionalized with respect to b_H = 3.0 feet and S_H = 6.18 square feet.

(b) Inverted T-configuration. Ratio of horizontal span to vertical span, 1.0; aspect ratio of horizontal surface, 0.728. Nondimensionalized with respect to b_H = 1.5 feet and S_H = 3.09 square feet.

Figure 5.- Effect of change of angle of attack on the sideslip derivatives of two representative configurations.

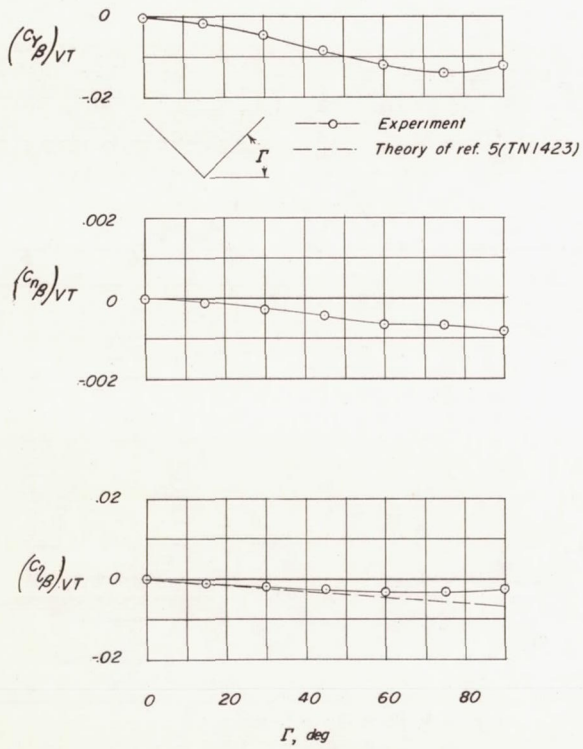

Figure 6.- Effect of change of dihedral angle on the sideslip derivatives for a delta configuration of aspect ratio 1.456. b = 3.0 feet; S = 6.18 square feet.

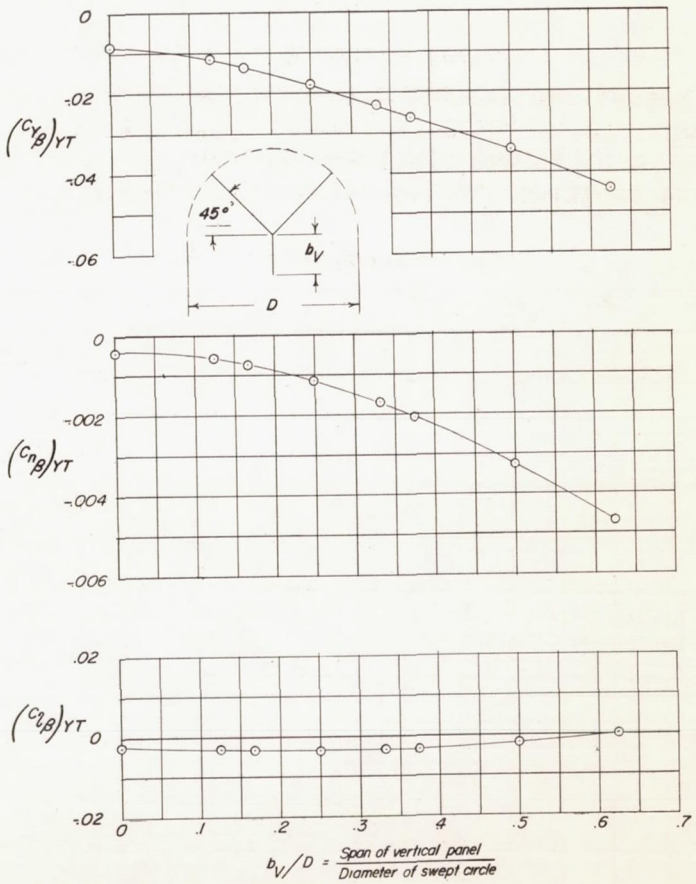

Figure 7.- Effect of change of ratio of the vertical span to the diameter of the circle swept by the other two spans on the sideslip derivatives for a series of Y-configurations. b = 3.0 feet; S = 6.18 square feet.

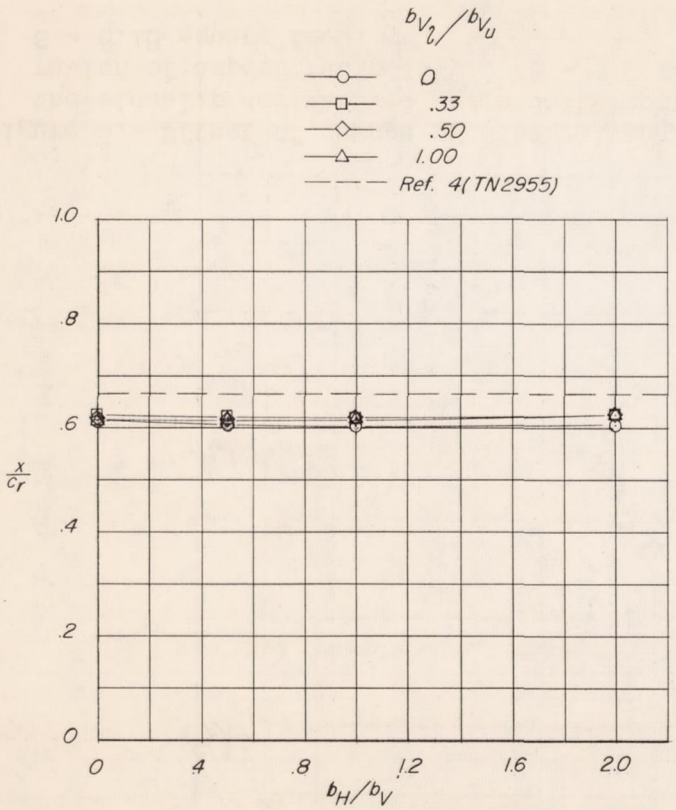

(a) Cruciform and inverted T-configurations. $\alpha = 0^{\circ}$.

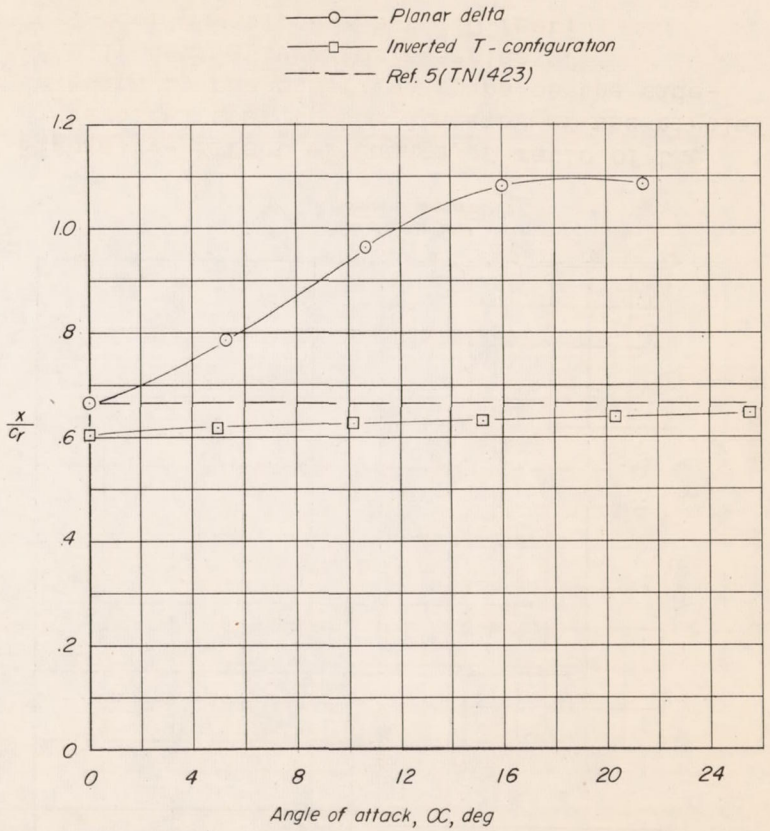

(b) Delta and inverted T-configurations through angle-of-attack range.

Figure 8.- Location of lateral-force center of pressure for the various configurations tested in sideslip.

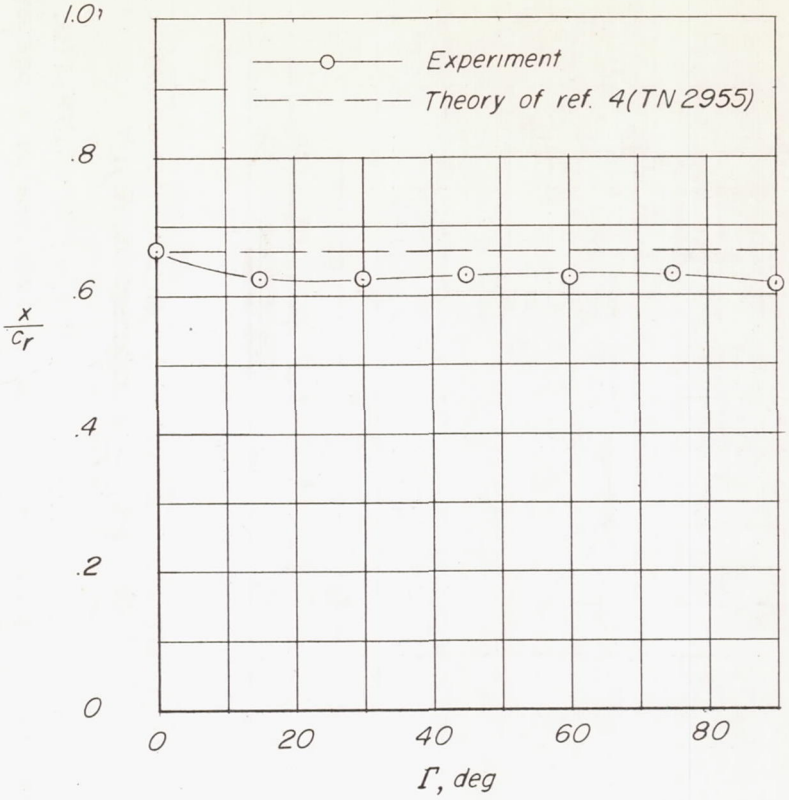

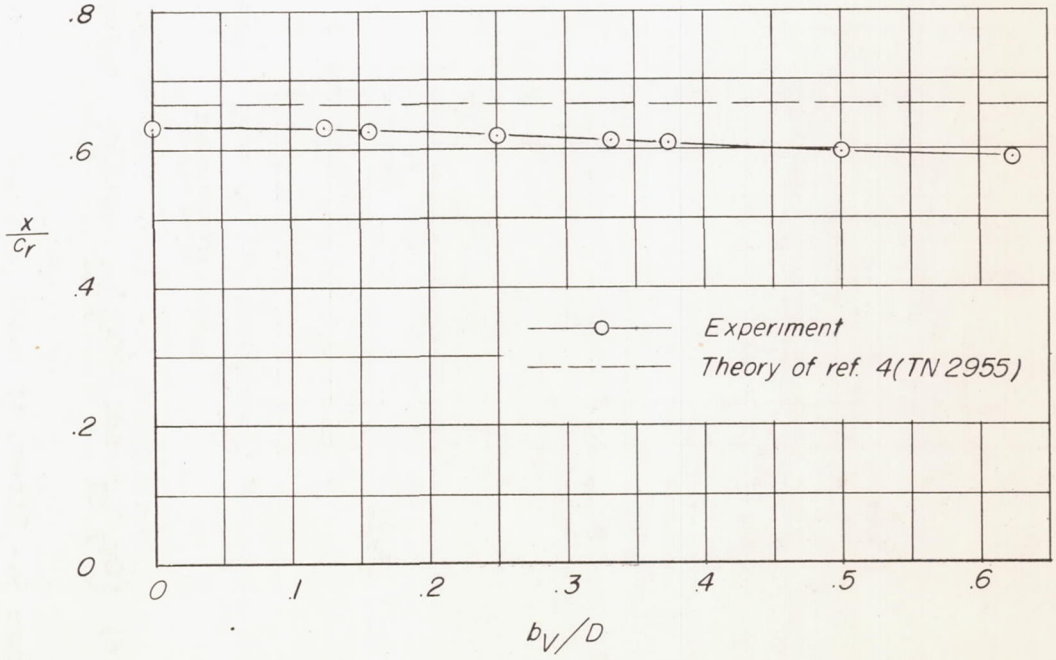

(c) V- and Y-configurations. $\alpha = 0^{\circ}$.

Figure 8.- Concluded.

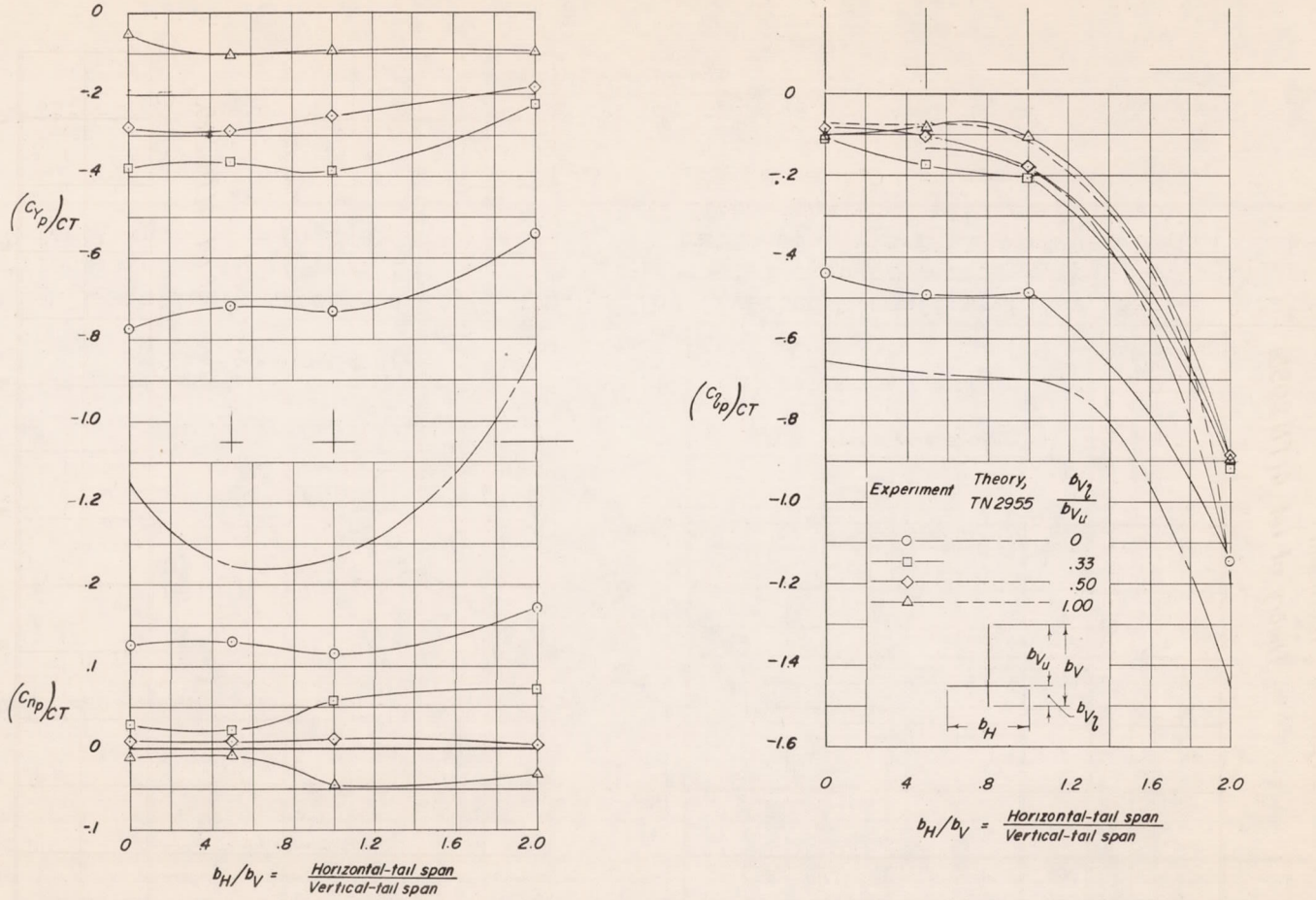

(a) $(C_{Y_p})_{CT}$ and $(C_{n_p})_{CT}$ against b_H/b_V.

(b) $(C_{l_p})_{CT}$ against b_H/b_V.

Figure 9.- Effect of ratio of lower to upper vertical span on the rolling derivatives of a series of cruciform configurations. b_V = 1.5 feet; S_V = 3.09 square feet.

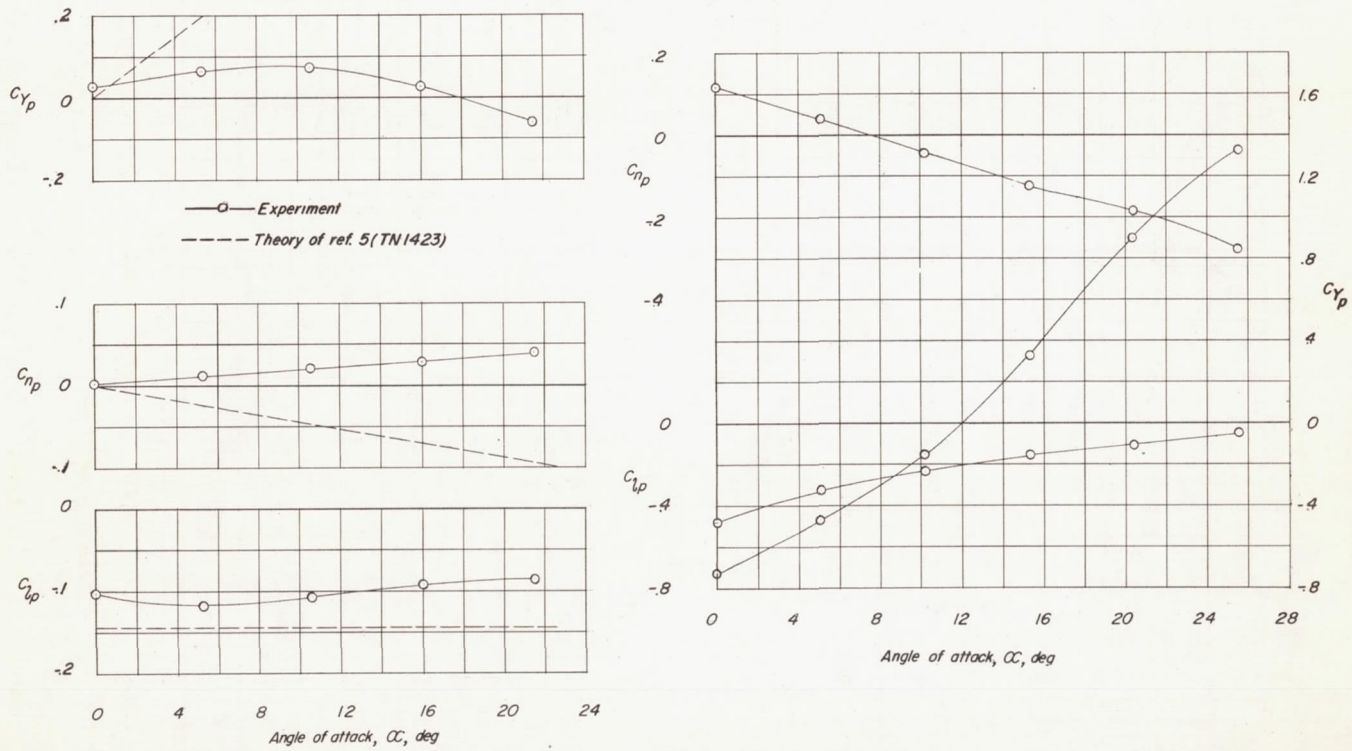

(a) Planar configuration. Aspect ratio, 1.456. Nondimensionalized with respect to b_H = 3.0 feet and S_H = 6.18 square feet.

(b) Inverted T-configuration. Ratio of horizontal span to vertical span, 1.0; aspect ratio of horizontal surface, 0.728. Nondimensionalized with respect to b_H = 1.5 feet and S_H = 3.09 square feet.

Figure 10.- Effect of change of angle of attack on the rolling derivatives of two representative configurations.

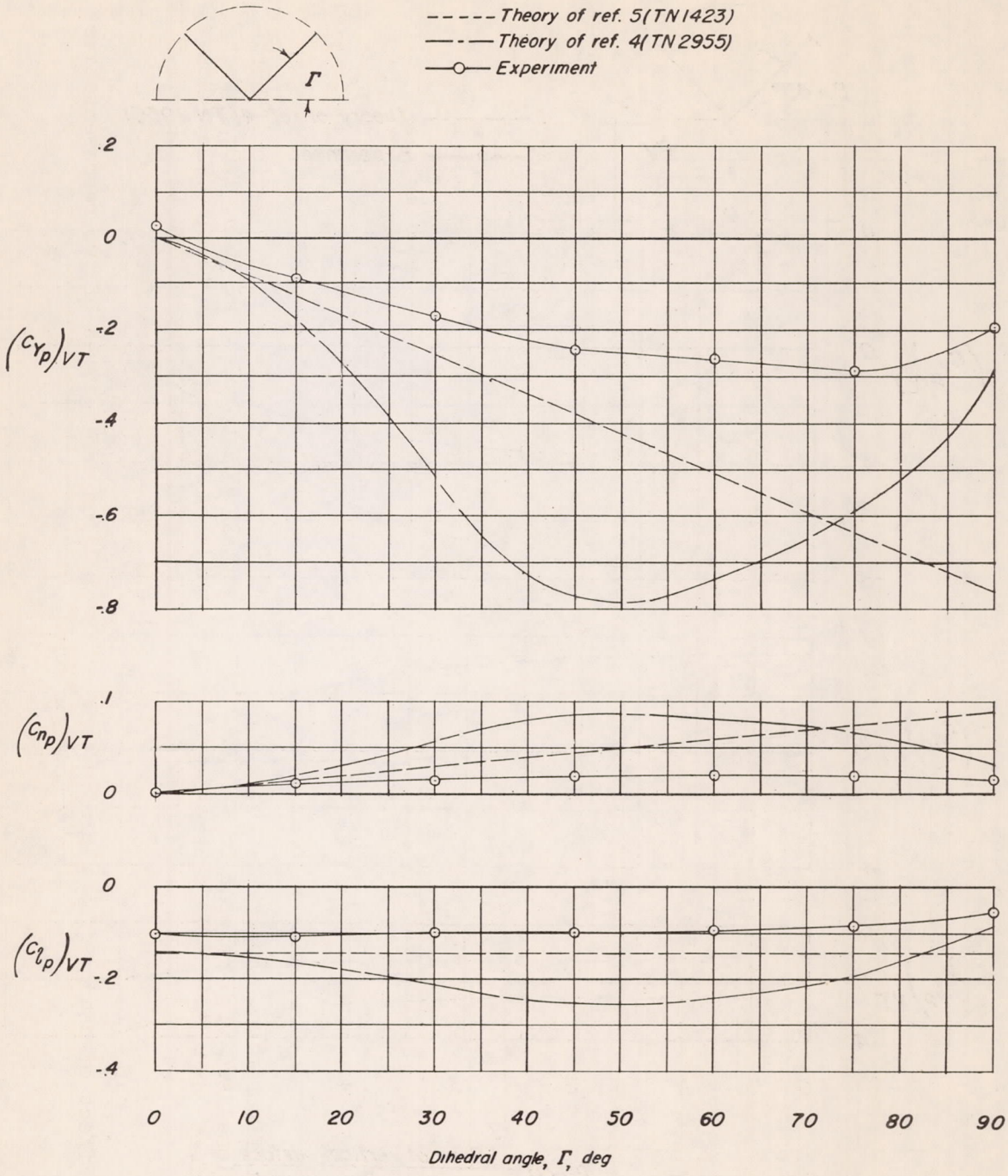

Figure 11.- Effect of change of dihedral angle on the rolling derivatives for a delta configuration of aspect ratio 1.456. b = 3.0 feet; S = 6.18 square feet.

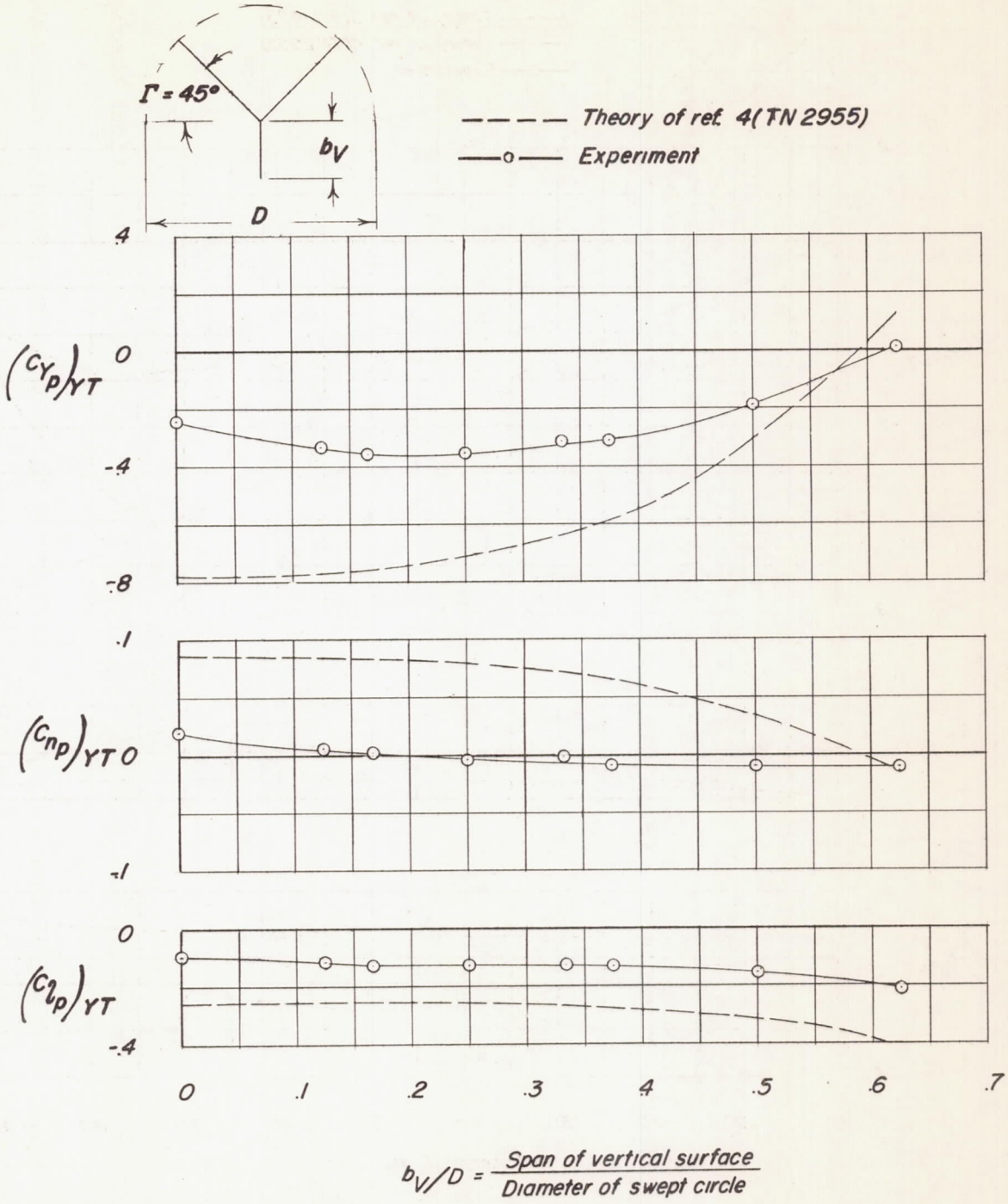

Figure 12.- Effect of change of ratio of the vertical span to the diameter of the circle swept by the other two spans on the rolling derivatives for a series of Y-configurations.

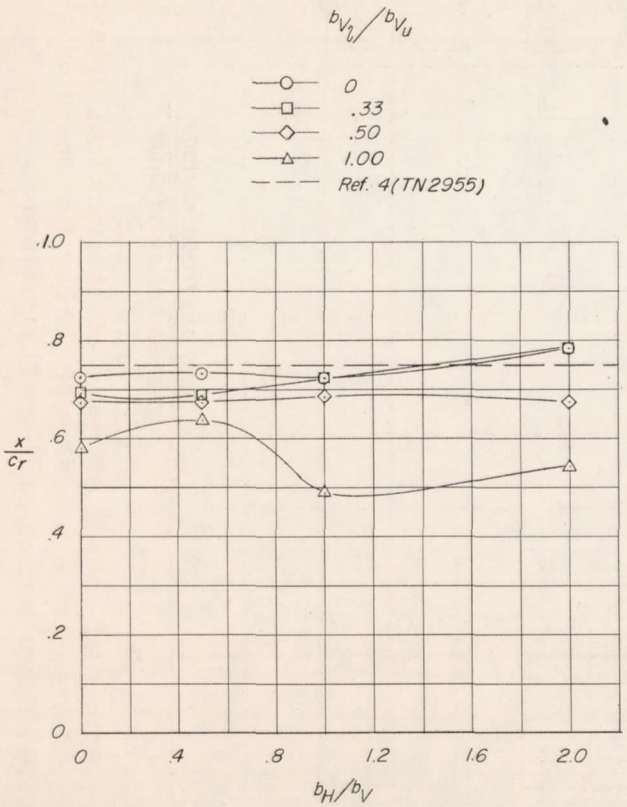

(a) Cruciform and inverted T-configurations. $\alpha = 0^{\circ}$.

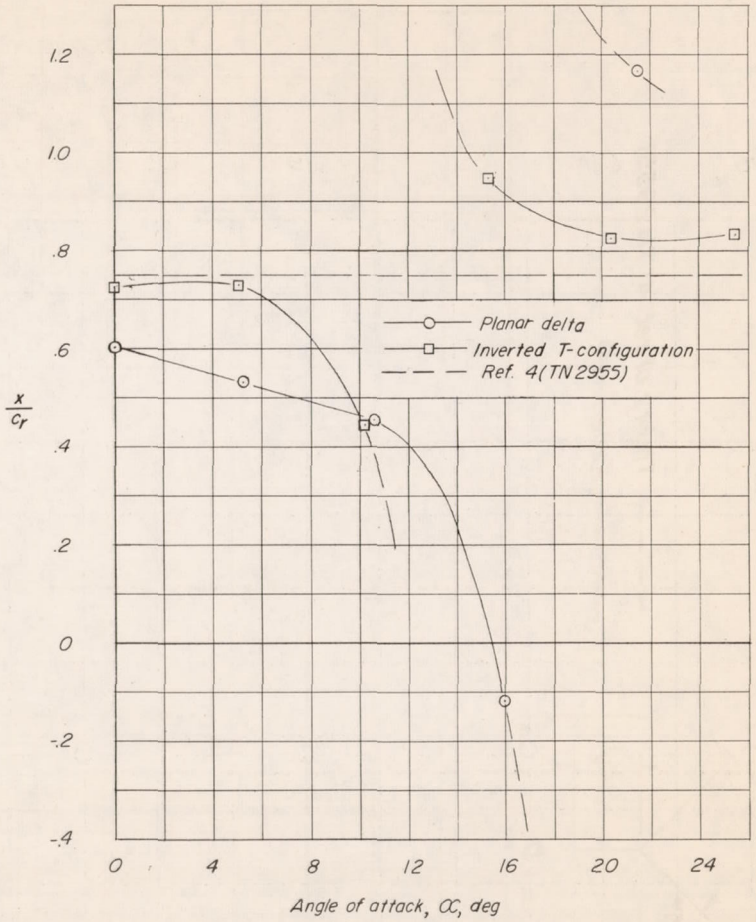

(b) Delta and inverted T-configurations through angle-of-attack range.

Figure 13.- Location of lateral-force center of pressure for the various configurations tested in rolling flow.

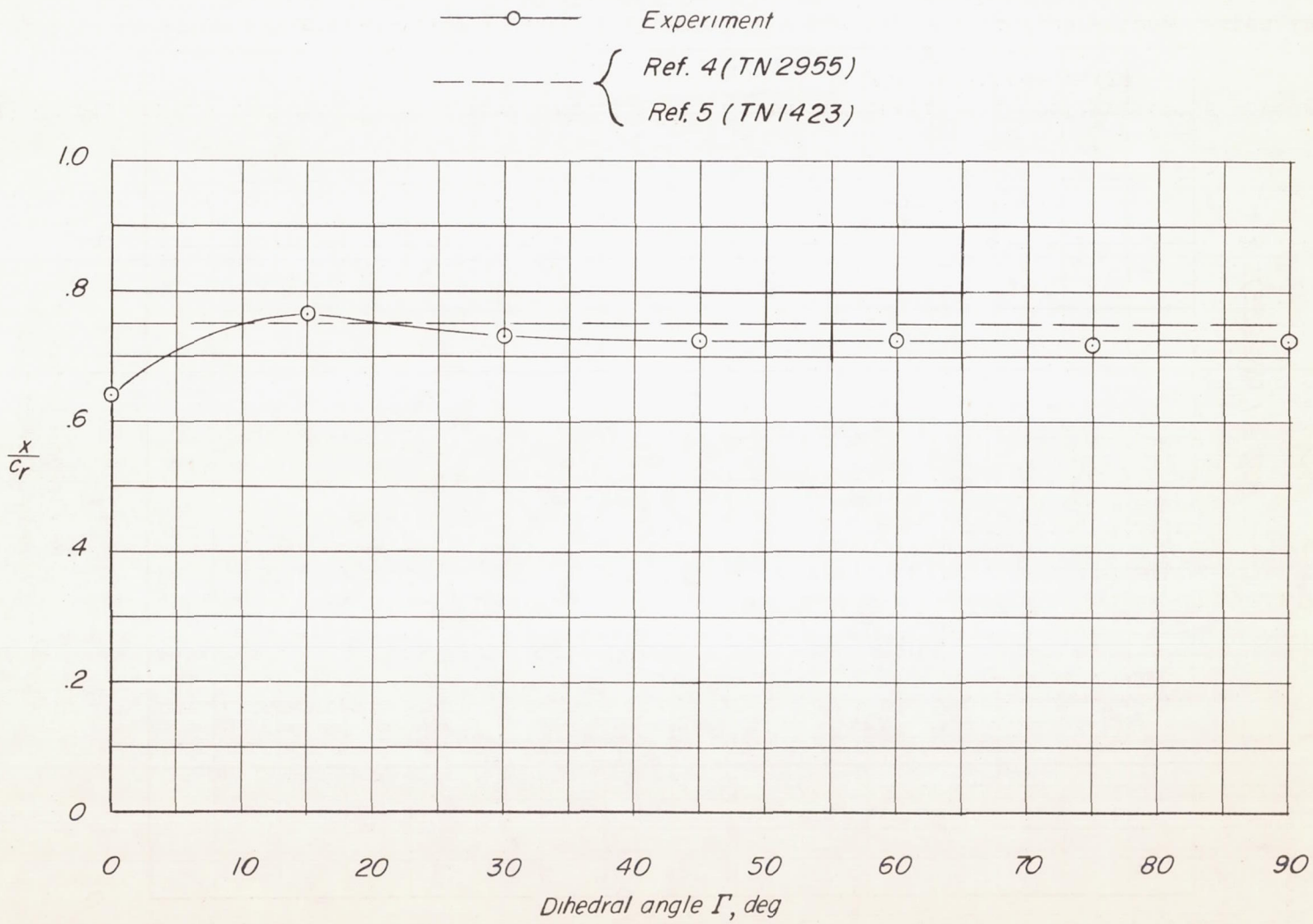

(c) V-configuration. $\alpha = 0^{\circ}$.

Figure 13.- Continued.

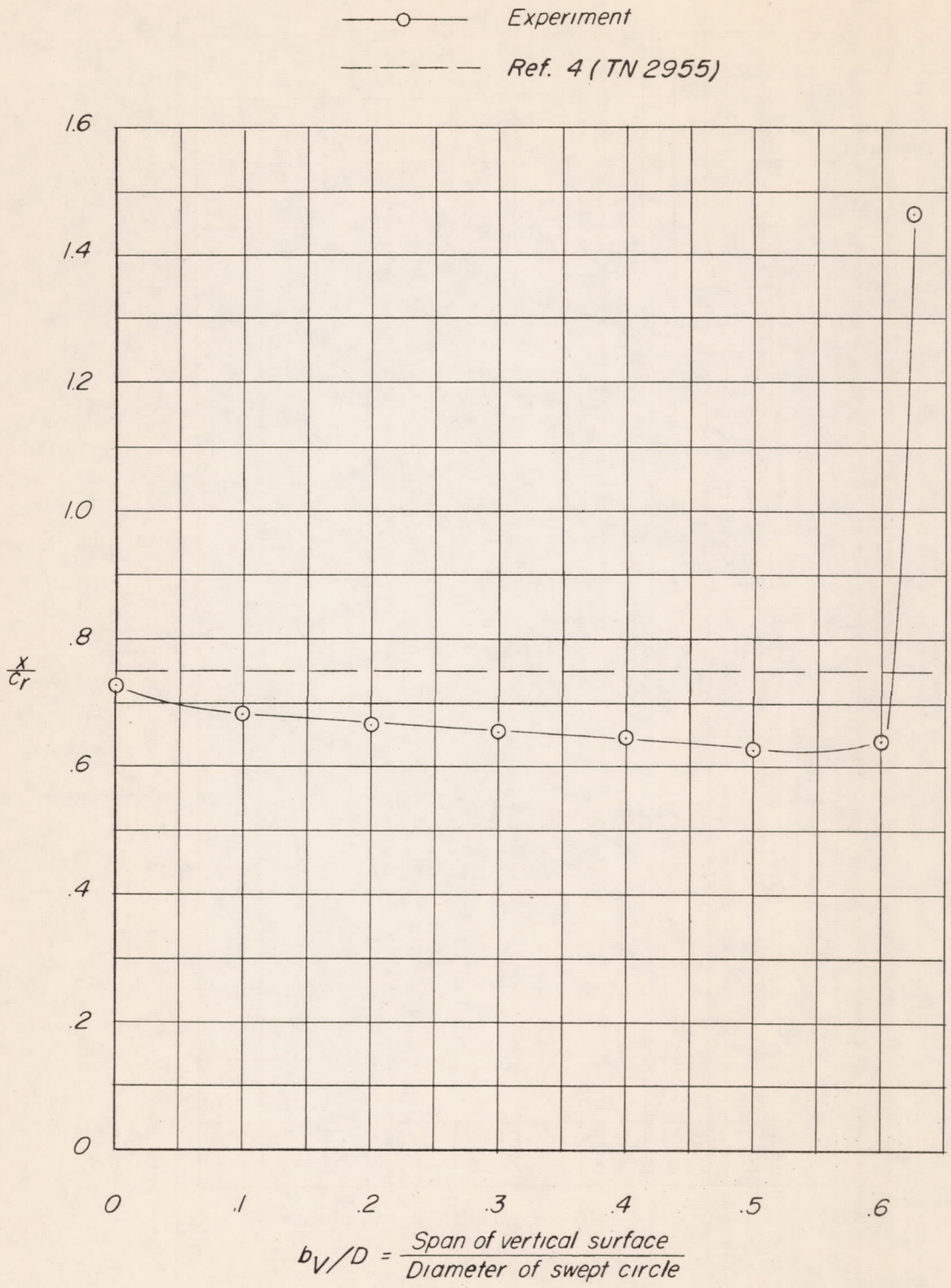

(d) Y-configuration. $\alpha = 0^{\circ}$.

Figure 13.- Concluded.